Target-Based Identification of Whole-Cell Active Inhibitors of Biotin Biosynthesis in *Mycobacterium tuberculosis*

Sae Woong Park,[1,6] Dominick E. Casalena,[2,6] Daniel J. Wilson,[3] Ran Dai,[4] Partha P. Nag,[2] Feng Liu,[4] Jim P. Boyce,[5] Joshua A. Bittker,[2] Stuart L. Schreiber,[2] Barry C. Finzel,[4] Dirk Schnappinger,[1,*] and Courtney C. Aldrich[3,4,*]

[1]Department of Microbiology and Immunology, Weill Cornell Medical College, New York, NY 10065, USA
[2]The Broad Institute Probe Development Center, Cambridge, MA 02142, USA
[3]Center for Drug Design, University of Minnesota, Minneapolis, MN 55455, USA
[4]Department of Medicinal Chemistry, University of Minnesota, Minneapolis, MN 55455, USA
[5]Division of Microbiology and Infectious Diseases, National Institute of Allergy and Infectious Diseases, National Institutes of Health, Bethesda, MD 20892-6604, USA
[6]Co-first author
*Correspondence: dis2003@med.cornell.edu (D.S.), aldri015@umn.edu (C.C.A.)
http://dx.doi.org/10.1016/j.chembiol.2014.11.012

SUMMARY

Biotin biosynthesis is essential for survival and persistence of *Mycobacterium tuberculosis* (*Mtb*) in vivo. The aminotransferase BioA, which catalyzes the antepenultimate step in the biotin pathway, has been established as a promising target due to its vulnerability to chemical inhibition. We performed high-throughput screening (HTS) employing a fluorescence displacement assay and identified a diverse set of potent inhibitors including many diversity-oriented synthesis (DOS) scaffolds. To efficiently select only hits targeting biotin biosynthesis, we then deployed a whole-cell counterscreen in biotin-free and biotin-containing medium against wild-type *Mtb* and in parallel with isogenic *bioA Mtb* strains that possess differential levels of BioA expression. This counterscreen proved crucial to filter out compounds whose whole-cell activity was off target as well as identify hits with weak, but measurable whole-cell activity in BioA-depleted strains. Several of the most promising hits were cocrystallized with BioA to provide a framework for future structure-based drug design efforts.

INTRODUCTION

Tuberculosis (TB) is an infectious disease caused by *Mycobacterium tuberculosis* (*Mtb*) and related species that is most commonly observed as a chronic pulmonary infection (World Health Organization (WHO), 2013). TB, once the leading cause of infectious disease mortality, was nearly eradicated from industrialized nations in the 20th century through a combination of public health measures and the introduction of antibiotics (Centers for Disease Control and Prevention (CDC), 1999). However, the emergence of HIV that sensitizes latently TB-infected individuals and the inevitable development of drug-resistant TB strains through use of the same antibiotics for more than 50 years has led to a dramatic worldwide rise in TB mortality, which prompted the WHO to declare TB a global public health emergency. Current efforts to bring TB under control are focused on development of new antibiotics, improved diagnostics, and vaccines (NIH, 2014). Ultimately, success in each area is required to control TB.

The development of new antibiotics for TB traditionally has been performed by empirically screening compound collections and natural product extracts for in vitro antitubercular whole-cell activity without any a priori knowledge of their mechanism of action (MOA) (Aldrich et al., 2010; Marriner et al., 2011). Streptomycin, the very first antibiotic effective against *Mtb* discovered by Albert Schatz in Selman Waksman's laboratory at Rutgers in 1943, and bedaquiline, the newest TB drug developed by Koen Andries' team at Janssen Pharmaceuticals and approved by the FDA for multidrug-resistant-TB in 2012, were discovered in this manner (Andries et al., 2005; Schatz et al., 1944). An inverse and potentially more intellectually appealing strategy for antibiotic discovery is to identify a target essential for growth (or survival) of the pathogen by comparative genomics and metabolic-pathway analysis and then search for an inhibitor.

Target-based approaches have been immensely successful for antiviral drug discovery; however, they have been much less effective in the antibacterial arena for many reasons (Gopal and Dick, 2014; Payne et al., 2007; Silver, 2011). One of the most significant challenges has been the inability to translate potent biochemical activity into whole-cell antibacterial activity. Moreover, many compounds with cell-based activity that were identified with biochemical assays may be found later to not act through inhibition of the intended target. To overcome these limitations, target-based whole-cell screening (TBWCS), which combines the specificity of biochemical target-based approaches with the practical advantages of whole-cell phenotypic screens to identify cell-permeable target-directed compounds, has been developed (DeVito et al., 2002; Forsyth et al., 2002; Young et al., 2006). In this approach, a target is differentially expressed in the bacterial cell, which potentially sensitizes the biochemical pathway to inhibition, and counterscreening enables one to deselect compounds that retain
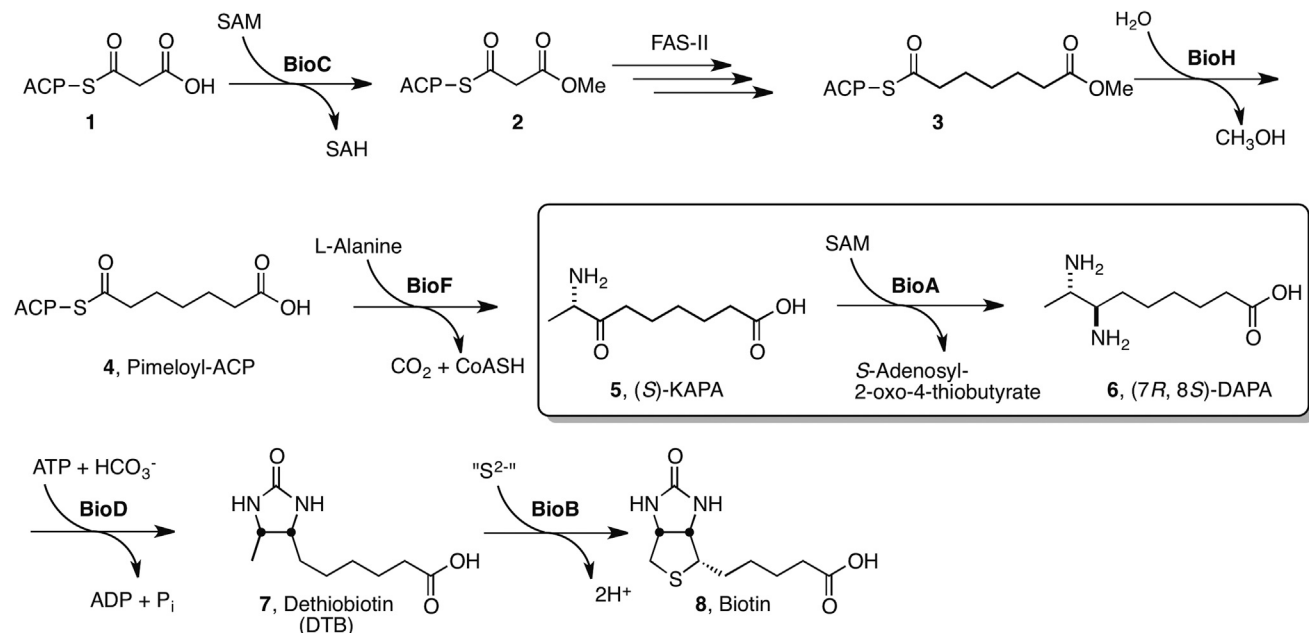
Figure 1. The Biotin Biosynthetic Pathway in Mtb

The biochemical pathway for biotin synthesis in analogy to the pathway in *Escherichia coli* is expected to proceed by methylation of malonyl-ACP 1 to the corresponding methyl ester 2 by BioC, which allows it to enter the fatty acid synthesis pathway (FAS-II) where it undergoes two rounds of extension to pimeloyl-ACP methyl ester 3 (Lin et al., 2010; Shapiro et al., 2012). Hydrolysis of the methyl ester 3 by BioH is expected to furnish pimeloyl-ACP 4. Next BioF catalyzes the decarboxylative condensation of pimeloyl-ACP 4 with alanine to furnish KAPA 5. Reductive amination of KAPA to DAPA 6 is performed by the PLP-dependent aminotransferase BioA. Carboxylation of DAPA 6 to dethiobiotin 7 mediated by BioD followed by C-H activation and sulfur insertion by BioB affords biotin 8.

activity presumably through alternate mechanisms. These strategies have been used successfully to identify new antibacterials for Gram-positive bacteria (Phillips et al., 2011; Wang et al., 2006) and recently were applied for the first time to *Mtb* (Abrahams et al., 2012).

We have genetically validated biotin biosynthesis as a promising pathway in *Mtb* that is essential for replication and persistence in vivo (Park et al., 2011). The biotin pathway is absent in higher organisms; thus, inhibitors of this pathway are expected to be intrinsically selective. BioA is a 5′-pyridoxal phosphate (PLP)-dependent aminotransferase that is responsible for the antepenultimate step of biotin biosynthesis (Figure 1), and it catalyzes the reductive amination of 7-keto-8-aminopelaragonic acid (KAPA, 5) to 7,8-diaminopelargonic acid (DAPA, 6), uniquely employing *S*-adenosyl-L-methionine (SAM) as the amino donor (Mann et al., 2009; Mann and Ploux, 2006, 2011). The natural product antibiotic amiclenomycin disrupts biotin metabolism in *Mtb* through inhibition of BioA and possesses remarkably selective antimycobacterial activity, thereby providing chemical validation for this pathway (Kitahara et al., 1975; Sandmark et al., 2002). However, the chemical instability and highly polar nature of this compound precludes its use in vivo (Shi et al., 2011). The chemical precedence provided by amiclenomycin in conjunction with our successful fragment-screening campaign supports the vulnerability of *Mtb* to chemical inhibition of BioA (Dai et al., 2014; Edfeldt et al., 2011).

Herein we report the identification of potent BioA inhibitors by screening the Molecular Libraries Small Molecules Repository (MLSMR) compound collection of more than 350,000 compounds using an innovative screening approach. A major challenge in hit discovery programs with biochemical assays is selecting compounds for further development, since a typical hit rate of 0.1%–0.3% on a library of this size can provide hundreds to thousands of confirmed hits with low micromolar activity. To rapidly identify compounds that operate through the desired MOA, we used a whole-cell counterscreen with wild-type (WT) *Mtb* in biotin-free and biotin-containing medium as well as BioA under- and overexpressing *Mtb* strains. Integration of the resulting whole-cell activity profiles enabled rapid selection of compounds with BioA-specific whole-cell activity. Moreover, the susceptible BioA-depleted *Mtb* strain allowed identification of compounds with modest, on-target whole-cell activity that would have been missed by enlisting only a WT *Mtb* strain. Several of the most promising scaffolds were cocrystallized with BioA and provide a foundation for future structure-based drug design studies.

RESULTS

Continuous Coupled Assay

To identify BioA inhibitors, we used a coupled assay under initial velocity conditions as shown in Figure 2, wherein the BioA product DAPA was converted into dethiobiotin by BioD (Mann et al., 2013; Wilson et al., 2011). The BioA substrates KAPA and SAM were held at 3 μM and 0.75 mM, respectively, which is near their K_M values, to provide balanced assay conditions (Copeland, 2000). Additionally, we used 1 mM dithiothreitol (DTT) to prevent false positives caused by thiol-reactive
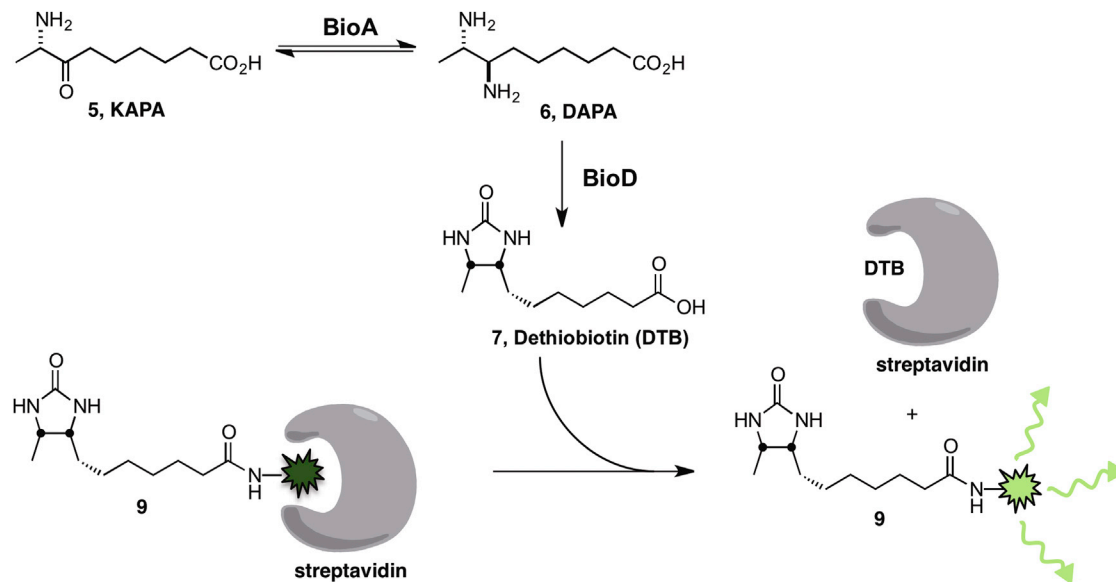
Figure 2. Overview of the Coupled Fluorescent Displacement Assay to Measure BioA Activity

BioA catalyzes the reversible transamination of KAPA 5 to DAPA 6, which is converted by BioD to dethiobiotin 7. Displacement of the fluorescently labeled dethiobiotin tracer 9 from streptavidin by the generated dethiobiotin 7 relieves the fluorescent quenching of 9 due to the tryptophan-rich environment of streptavidin (W79, W92, W108, and W120). The depicted binding of streptavidin to 7 and 9 does not accurately portray the molecular interactions. Streptavidin can bind four molecules of dethiobiotin 7 in each of the four equivalent biotin-binding sites of the homotetramer, while the dethiobiotin and the fluorescein moieties of 9 are predicted to each occupy one of the four equivalent biotin-binding sites (Wilson et al., 2011).

molecules and 0.0025% Igepal CA630, a nonionic detergent, to impede nonspecific inhibitor aggregation (McGovern et al., 2003). The use of BioD drives the overall reaction forward since the aminotransferase reaction is reversible. Detection of dethiobiotin was achieved with streptavidin and a fluorescently labeled tracer that we developed, whose fluorescence quenching is relieved upon displacement by dethiobiotin (Wilson et al., 2011). Termination of the assay was accomplished by the addition of a 500 mM EDTA solution, which chelates the Mg^{2+} cofactor required for BioD activity.

Assay Screen

The assay was miniaturized to a 7.5 μl 1,536-well format where it performed with a calculated Z′ factor of 0.825 ± 0.103, which is a measure of assay robustness (Zhang et al., 1999). Screening was performed in duplicate at a single concentration of 10 μM against the MLSMR collection of 356,486 diverse compounds (PubChem AID 602481). Notably, this library includes 83,000 compounds from the diversity-oriented synthesis (DOS) compound collection at the Broad Institute. We defined a hit as a compound showing greater or equal to 40% inhibition, and 342 compounds were active at 10 μM by this criteria, representing a nominal hit rate of 0.095% (Figure 3). Hits were triaged to remove most pan assay interference compounds (Baell and Holloway, 2010), yielding 327 hits of which 312 were available for retesting. Retesting was performed in an eight-point concentration-response format in triplicate, and 298 of the 312 hits possessed IC_{50} values ≤ 20 μM with 55 compounds exceeding the activity threshold of IC_{50} ≤ 1 μM, giving a confirmation rate of 96% (PubChem AID 651683) (see Figure S1 for assay tree, available online).

Secondary Assays

Next, all 298 hits were counterscreened in an eight-point dose-response format against BioD, using the substrate DAPA along with streptavidin and the fluorescent dethiobiotin tracer to identify compounds that cause fluorescence interference or inhibit BioD (PubChem AID 651679). None of the hits showed activity in the BioD counterscreen (IC_{50} > 20 μM). Since BioA is a PLP-dependent aminotransferase and because previous BioA inhibitors have been shown to covalently bind the PLP cofactor, we evaluated all compounds against aspartate transaminase (AST), an ubiquitous and functionally related PLP-dependent enzyme, to assess potential enzyme selectivity (AID 743184; Dai et al., 2014; Sandmark et al., 2002; Shi et al., 2011; Zlitni et al., 2013). All of the hits were inactive against AST, suggesting they possess a useful level of selectivity. To evaluate the potential for mammalian cytotoxicity, every hit was then screened against HepG2 human liver cells, HEK293 human kidney cells, and NIH 3T3 murine fibroblast cells; none of the 298 hits demonstrated any cytotoxicity at 20 μM, the maximum compound concentration evaluated (PubChem AID 651898, AID 651899, and AID 651900), and all were carried forward for further study.

Scaffold Analysis

Cheminformatic analysis followed by manual culling of the 298 confirmed hits suggested chemical clustering into 65 groups, of which 34 groups were defined by multiple examples sharing a common scaffold (Table S1) (Mulrooney et al., 2013). Tetrahydroisoquinoline 10, from a DOS library and shown in Table 1, is the most abundant scaffold (36 analogs), representing nearly 12% of all hits and including the most potent hit identified with an IC_{50} value of 75 nM (Gerard et al., 2012). Another interesting
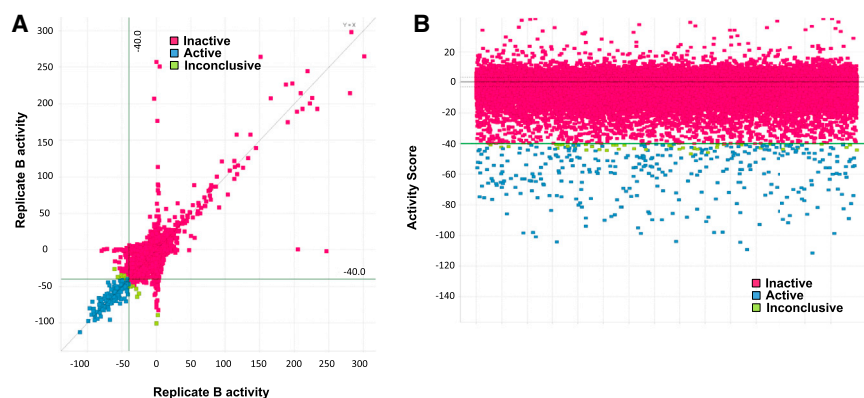
Figure 3. Summary of Data from All >350,000 Wells of the Entire MLSMR Library Screen
(A) Replicate comparison plot of screened compounds. Activity of 0 represents the average of the DMSO neutral control wells and of −100 the average of the positive control wells. Compounds with all replicates passing the −40% activity score threshold are considered active (blue), those with the mean of the replicates above −40% are considered inactive (red), and those with a mean replicate activity below −40% but with less than half the replicates passing the threshold are inconclusive (green).
(B) Mean activities of all replicates for each compound. Coloring and activity calls are as in (A). The −40% activity threshold is shown.

DOS scaffold (6 analogs) is the oxazocane typified by 17 (Gerard et al., 2013). Several other DOS scaffolds registered as hits (Table S1), including benzooxathiazocines (Gerard et al., 2011), monocyclic azetidine nitriles (Lowe et al., 2012), and tricyclic pyridones (Marcaurelle et al., 2009).

Several other chemotypes were identified with promising biological activity, among these 5,6-fused bicyclic heteroaromatics were the third most common scaffold (23 analogs) and pyrazolo[1,5-*a*]pyrimidine 11 is shown as an example. The piperidines (20 analogs) typified by 16, constituted the fourth most populous scaffold. The *N*-aryl piperazines, such as 14, represented the fifth most abundant scaffold (16 analogs). The coumarins, exemplified by 7-diethylaminocoumarin 15, were the sixth most abundant scaffold. Additionally, several other small clusters of two to three compounds demonstrated promising BioA inhibitory activity with pyrrolothiazolidine-*S*-oxide 18 and benzimidazole 19 provided as representative molecules. Among the compounds with no clear chemical analogs in the screening libraries were examples like phthalazinone 12 and 4-(benzothiazol-2-yl)pentenoic acid 13.

Whole-Cell Evaluation
Representative members of each scaffold were evaluated against *M. tuberculosis* H37Rv in biotin-free and biotin-containing medium to identify compounds with biotin-dependent *Mtb* growth inhibitory activity. Additionally, compounds were tested against an *Mtb* strain that expresses approximately 20% of BioA relative to WT *Mtb* and, therefore, is sensitive to BioA inhibition. This strain was originally described as BioA TetON-5 (Park et al., 2011) and is referred to here as BioA-underexpressor or BioA-UE. Select compounds were then screened against an *Mtb* strain that expresses approximately 1,200% of BioA relative to WT *Mtb* and, thus, should be more resistant to putative BioA inhibitors. The overexpressor was described as Bio TetON-1 (Park et al., 2011) and is referred to here as BioA-OE. The results from these whole-cell screens allowed prioritization of hits based on on-target whole-cell activity.

The utility of this approach is illustrated with *N*-aryl piperazine 14 (Figure 4A), which showed modest activity against WT *Mtb* with a minimum inhibitory concentration (MIC) that inhibited 90% of growth at 26 μM in biotin-free medium. Addition of 1 μM biotin to the medium blocked the activity of 14 and chemically rescued the bacteria. Depletion of BioA in *Mtb*

BioA-UE increased susceptibility to 14, yielding an MIC of 9 μM, while BioA overexpression in *Mtb* BioA-OE conferred resistance to 14, shifting the MIC to 99 μM. Collectively, these results are consistent with the desired MOA and present *N*-aryl piperazine 14 as a validated hit, which we will report on further in the future.

In a similar manner, this screening approach can be used to invalidate hits even though they may otherwise appear promising based on their biochemical and whole-cell activity. This is illustrated with 4-(benzothiazol-2-yl)pentenoic acid 13, which was the most potent whole-cell active hit identified with an MIC against WT *Mtb* of 2.5 μM in the absence of biotin. However, the MIC was only modestly shifted (approximately 3-fold) to 8.7 μM upon addition of biotin, suggesting the activity was largely biotin-independent. Assay of 13 using strains that under- or overexpressed BioA provided MICs of 0.7 and 4.7 μM, respectively. These MICs were relatively insensitive to BioA levels, which varied 60-fold between strains BioA-UE and BioA-OE (Park et al., 2011). Thus, while 4-(benzothiazol-2-yl)pentenoic acid 13 had promising biochemical activity (IC_{50} = 153 nM), the observed whole-cell antimycobacterial activity showed lesser dependence on exogenous biotin or BioA protein levels, suggesting that the observed whole-cell activity was primarily due to off-target effects. Consequently, hit 13 was deprioritized for further development.

A third set of compounds was also identified from this screening method as exemplified by pyrrolothiazolidine-*S*-oxide 18, whose MIC against WT *Mtb* in biotin-free medium was greater than 50 μM. Compound 18 showed no observable growth inhibition in biotin-containing medium or against the BioA overexpression strain. In most screening work flows this compound would be discarded. However, activity was revealed when this compound was evaluated against the sensitive strain BioA-UE, wherein BioA is depleted relative to WT, providing an MIC value of 35 μM, which warrants further investigation. Several other hits also demonstrated weak whole-cell activity against BioA-UE, but are inactive against the other *Mtb* strains and growth conditions including pyrazolo[1,5-*a*]pyrimidine 11, piperidine 16, and DOS oxazocane 17 (see Table S1 for all active compounds).
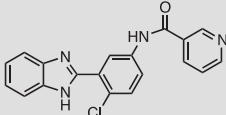
The majority of the 255 hits showed no activity against any of the *Mtb* strains, which is in agreement with prior observations of biochemical screening campaigns (Payne et al., 2007;

Table 1. Selected BioA and Mtb Hits

Compound	Structure	IC$_{50}$, μM[a]	MIC$_{90}$, μM BioA-UE[b]	MIC$_{90}$, μM WT -biotin[c]	MIC$_{90}$, μM WT+biotin[d]	MIC$_{90}$, μM BioA-OE[e]
10		0.075	>100	>100	>100	>100
11		0.144	15.1	75.1	>100	57.8
12		0.148	79.3	>100	>100	>100
13		0.153	0.7	2.5	8.7	4.7
14		0.155	9.3	26.3	>100	98.6
15		0.195	5.6	20.7	65.0	77.9
16		0.508	35.0	>100	>100	>100
17		0.596	98.7	>100	>100	>100
18		0.659	34.9	>100	>100	>100

Table 1. *Continued*

Compound	Structure	IC$_{50}$, µM[a]	MIC$_{90}$, µM BioA-UE[b]	MIC$_{90}$, µM WT -biotin[c]	MIC$_{90}$, µM WT+biotin[d]	MIC$_{90}$, µM BioA-OE[e]
19		0.788	14.5	46	72.9	39.5

Full data are available in PubChem (go to http://pubchem.ncbi.nlm.nih.gov/# and search under the bioassay tab with the given six-digit AID number).
[a]IC$_{50}$ value against *Mtb* BioA in the described biochemical assay: AID 651683.
[b]Minimum inhibitory concentration that results in 90% inhibition against the *Mtb* BioA underexpression strain: AID 743072 and AID 743352.
[c]Minimum inhibitory concentration that results in 90% inhibition against *Mtb* H37Rv without supplemental biotin: AID 743070 and AID 743350.
[d]Minimum inhibitory concentration that results in 90% inhibition against *Mtb* H37Rv with 1 µM supplemental biotin: AID 743071 and AID 743349.
[e]Minimum inhibitory concentration that results in 90% inhibition against the *Mtb* BioA overexpression strain: AID 743073 and AID 743351.

Silver, 2011), and these hits can be rapidly deprioritized without expending chemistry-intensive resources.

Structural Characterization

To facilitate future structure-based drug design, seven of the most promising hits were subjected to cocrystallization with BioA. Three complex structures were obtained including 7-diethylaminocoumarin 15, pyrrolothiazolidine-*S*-oxide 18, and an *N*-aryl piperazine 14-Cl, which is otherwise identical to hit *N*-aryl piperazine 14 except the dioxolane ring is replaced with a *meta*-chloro substituent. Unambiguous electron density affirmed that each inhibitor bound in the hydrophobic site adjacent to the PLP cofactor where substrate KAPA also bound, as shown in Figure 5 (Dai et al., 2014). This site exists at the interface of monomers in the BioA heterodimer; inhibitors are in contact with structural components of both monomers, distinguished by color in Figures 5A–5C. Each inhibitor induced shifts in the conformation of side chains of Tyr25 and Trp64 to accommodate the longer, flatter molecules that lie sandwiched between repositioned aromatic rings of the tyrosine below and the tryptophan above.

Interactions between these inhibitors and BioA are primarily hydrophobic and arise from two subsites. A subsite on the right (orientation defined by Figure 5) is formed by the juxtaposition of Pro24 and Trp 64 with residues 91'–93' and 316'–318' (primes denote residues of the other BioA monomer). The *m*-fluorophenyl group of 18, the thienyl ketone of 15, and the acetophenone group of 14-Cl all lie in this subsite, with the aromatic groups in planar coincidence. The fluorine of 18 is inserted most deeply into this subsite, where it is nestled between Gly'93 and Met'91. The acetocarbonyl of 14-Cl accepts an H-bond from the amide NH of Gly'93, the only H-bond donor or acceptor present in this otherwise hydrophobic pocket. A subsite on the left exists between the side chain of Tyr25, Tyr157, and the loop formed by Gly172-Met174. The subsite is capped by Arg403, although none of these inhibitors extend far enough to achieve direct contact with it. The chlorobenzyl of 14-Cl extends to the limit of this subsite, with the aromatic ring stacked in what could be a π-π interaction along the flat face of the peptide bond joining Gly173 and Gly173. Inhibitor 18 is too short to extend into this subsite. One branch of the diethylamine of 15 lies in a similar position, while the other branch

extends upward toward a niche between Tyr25 and Met174 not occupied by other inhibitors.

Inhibitor 18 is too short to contact the left subsite, but it is the only inhibitor that extends down to make direct contact with the PLP. The *S*-oxide of the pyrrolothiazolidine is positioned to donate an H-bond to one oxygen of the PLP phosphate and accept one from the hydroxyl group of Tyr157.

Isothermal Titration Calorimetry

To futher confirm the activity of *N*-aryl piperazine 14, we independently synthesized it (see Supplemental Experimental Procedures) and measured binding to BioA by isothermal titration calorimetry (ITC) (Figure 6). Consistent with our kinetic assay, 14 bound BioA tightly with a K_D of 110 ± 9 nM in a 1:1 stoichiometry. The affinity was enthalpically driven ($\Delta H = 11.8 ± 0.8$ kcal/mol) with a small unfavorable entropic component ($-T\Delta S = +2.8 ± 0.8$ kcal/mol).

DISCUSSION

Target-Based Strategies

Reductionist target-based approaches have gained considerable notoriety in antibacterial drug discovery because of their limited success (Payne et al., 2007; Silver, 2011). There are several potential reasons for the poor outcome of target-based strategies for antibacterial development, including the challenge of converting a biochemical inhibitor into a compound that leads to bacterial accumulation, rapid evolution of resistance to single targets, and the difficulty of developing broad-spectrum compounds. With respect to TB, narrow-spectrum agents that do not affect the commensal microbiota are in fact preferred, thus removing a major constraint typically faced by antibiotic discovery programs. The other major concern that has plagued antibiotic development is the high resistance frequencies of single-target agents, but this is less important for diseases like TB and HIV since combination drug therapy is always employed. For intracellular cytosolic targets in *Mtb*, which represent the majority of novel targets, the lack of efficacy of potent biochemical hits generally has been ascribed to a lack of penetration through the lipophilic cell envelope; however, drug efflux increasingly is being recognized as a major contributor to intrinsic resistance to antibiotics in *Mtb*. As recently demonstrated by Lee and
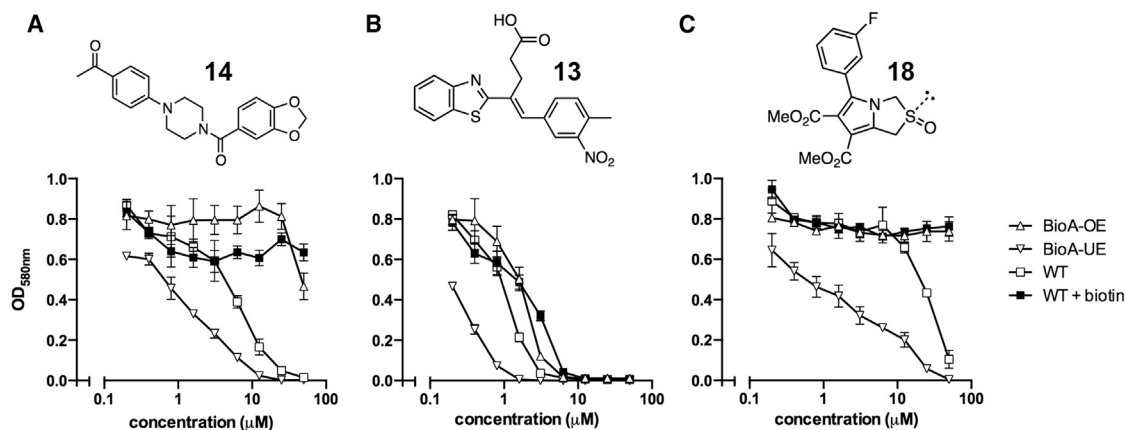
Figure 4. Whole-Cell Screening

(A–C) Whole-cell screening was performed with 120 compounds in WT *Mtb* in biotin-free and biotin-containing medium and BioA over- and underexpression strains, BioA-OE and BioA-UE, respectively. Examples of whole-cell screening with *N*-aryl piperazine 14 (A), 4-(benzothiazol-2-yl)pentenoic acid 13 (B), and pyrrolothiazolidine-*S*-oxide 18 (C) are shown. Error bars represent SD. Full data are available in PubChem AID 743070 and AID 743350 for WT *Mtb* in biotin-free medium, AID 743071 and AID 743349 for WT *Mtb* in biotin-containing medium, AID 743073 and AID 743351 for BioA-OE, and AID 743072 and AID 743352 for BioA-UE.

coworkers, efflux-pump-mediated resistance may be successfully overcome through chemical modification of the parent antibiotic scaffold (Lee et al., 2014). Based on the unique requirements for TB chemotherapeutic agents as noted above combined with the potential ability to overcome efflux-mediated resistance, target-based strategies could be well-suited for TB drug development.

TBWCS

Rudimentary TBWCS was first performed in the 1960s using pathway mutants in cell-wall biosynthesis (Silver, 2013). Modern TBWCS approaches employing antisense and siRNA target knockdown were reported by several groups (DeVito et al., 2002; Forsyth et al., 2002; Yin et al., 2004), and this led to the discovery of the antibiotics platensimycin and kibdelomycin (Phillips et al., 2011; Wang et al., 2006; Young et al., 2006). Mizrahi and coworkers were the first to apply TBWCS to *Mtb* and used a more sophisticated method with conditional mutants that underexpress essential genes for inhibitor screening, since antisense and siRNA methods are largely ineffective in *Mtb* (Abrahams et al., 2012). Our results extend these prior findings and highlight the utility of whole-cell studies with genetically modified strains for mode-of-action determination. Remarkably, the work flow described here identified selective biotin-dependent on-target compounds that inhibit growth of *Mtb*, even though BioA requires more than 95% depletion to affect growth (Park et al., 2011).

While TBWCS is gaining momentum, it is important to recognize the limitations of this approach, because sensitivity to antibiotics does not always monotonically increase with target expression levels (Palmer and Kishony, 2014). Thus, respective target underexpression in *E. coli* paradoxically reduces susceptibility to fluoroquinolines when the target DNA gyrase is underexpressed, and has no effect on the sulfonamide antibacterials when the target dihydropteroate synthase is underexpressed. As astutely noted by Palmer and Kishony, deviations from the expected monotonic relationship between sensitivity and target expression levels suggests more complex MOAs (Palmer and Kishony, 2014).

Promising Scaffolds

We identified and structurally characterized several inhibitors with interesting chemotypes that potently inhibit BioA and possess on-target whole-cell activity. The *N*-aryl piperazine scaffold of 14 is the most promising compound identified in this high-throughput screening (HTS) campaign, based on its chemical tractability for further development, potent biochemical activity (IC_{50} = 155 nM), and on-target biotin-dependent whole-cell activity. The cocrystal structure of this scaffold with BioA reveals several opportunities to enhance potency and selectivity. Additionally, several other meritorious scaffolds were identified using the sensitive BioA knockdown *Mtb* strain, including pyrazolopyrimidine 11, piperidine 16, and pyrrolothiazolidine-*S*-oxide 18. Coumarin 15 and benzimidazole 19 possess attractive biotin- and BioA-dependent whole-cell activity and lack cytotoxicity. However, their activity profiles indicate partial off-target activity as the activity was not eliminated upon BioA overexpression or addition of exogenous biotin. These compounds therefore warrant further study given their favorable therapeutic index and promising activity, but do not represent useful molecular scaffolds for preparation of a probe for in vivo chemical validation of biotin synthesis in *Mtb*.

Prior structural studies with *Mtb* BioA have clearly shown that the active site is highly adaptable in the presence of different bound ligands (Dai et al., 2014; Dey et al., 2010; Shi et al., 2011). This plasticity is not unexpected, given the need for the enzyme to recognize, bind, and catalyze chemical transformations of such diverse substrates as KAPA and SAM. Nevertheless, specific conformational changes that support ligand binding are not easily predicted a priori. Each of the high-resolution inhibitor complexes described here represents an induced protein conformation that constitutes a possible ground state
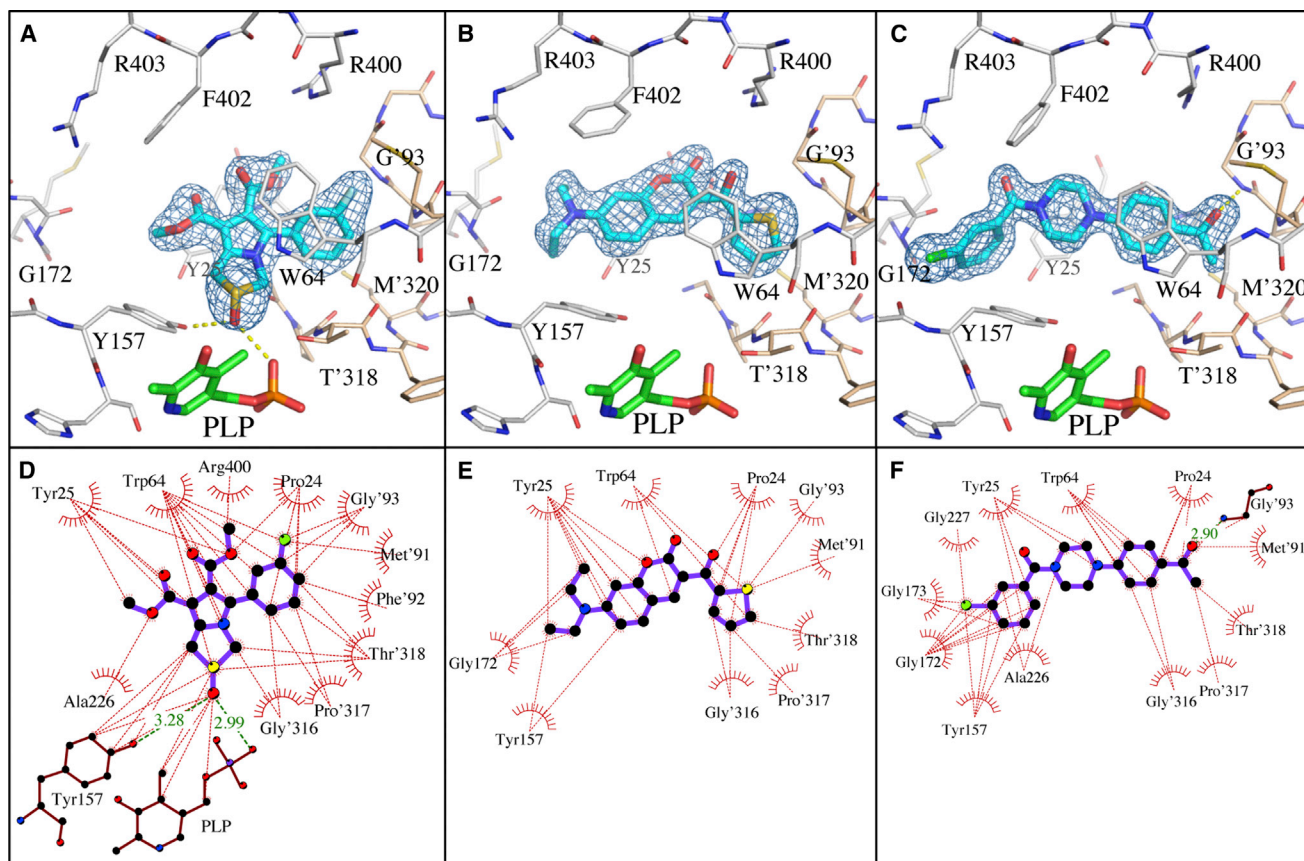
Figure 5. Crystal Structures with Bound Inhibitors

(A–C) 3σ omit density (F_o-F_c) from cocrystal structures of pyrrolothiazolidine-*S*-oxide 18 (A), 7-diethylaminocoumarin 15 (B) and *N*-aryl piperazine 14-Cl (C) (cyan), and the molecular environment surrounding the binding site near the PLP (green). Comparable binding is observed in both active sites of the BioA heterodimer, but only one is shown. Residues from one monomer are identified with primes; those from the other are not.

(D–F) Ligand interaction maps. Hydrogen bonds are shown as green dashed lines, and hydrophobic contacts (closer than 3.9 Å) are identified by thin red dashed lines.

for use in modeling or design of analogs derived from these scaffolds.

SIGNIFICANCE

Biotin biosynthesis is a genetically validated pathway in *Mtb* for antibiotic development. The chemical precedence and narrow-spectrum activity afforded by the antibiotic amiclenomycin, which inhibits biotin biosynthesis at BioA, highlight the unique vulnerability of this pathway in *Mtb*. Here we describe the identification of potent on-target BioA- and biotin-dependent *Mtb* whole-cell active compounds through HTS followed by phenotypic screening employing isogenic *Mtb* strains that differentially express BioA. The use of *Mtb* strains that allow modulation of BioA protein levels was crucial to distinguish among hits with nonspecific versus on-target activity. More importantly, the use of BioA-depleted *Mtb* strains revealed hits with on-target whole-cell activity that would be overlooked by traditional antibiotic discovery work flows. The structural characterization of three different scaffolds bound in the BioA active site

directly adjacent to the PLP-cofactor demonstrate the remarkable plasticity of BioA to accommodate structurally diverse ligands, which may account for the unique vulnerability of this target to chemical inhibition by a wide array of diverse chemical types.

EXPERIMENTAL PROCEDURES

Materials

BioA and BioD were expressed and purified as described previously (Geders et al., 2012; Wilson et al., 2011). The aspartate transaminase assay kit was purchased from BioAssay Systems. The fluorescent tracer N^1-{3-[2-(2-{3-[(fluorescein-5-yl)carbonyl]aminopropoxy}ethoxy)ethoxy]propyl}dethiobiotinamide 9 (Wilson et al., 2011); KAPA, 5 (Wilson et al., 2011); and DAPA,6 (Vasanthakumar et al., 2007) were synthesized as reported. Previously identified (Wilson et al., 2011) as a BioA inhibitor from screening the LOPAC library (Sigma-Aldrich), 6-(2-fluorophenyl)-1,3-dioxolo[4,5-*g*]quinolin-8(5H)-one (CHM-1) was used as a positive control and purchased from R&D Systems. All other buffers, salts, and reagents for the HTS assay (streptavidin from *Streptomyces avidiniii* as a salt-free lyophilized powder, *S*-(5′-adenosyl)-L-methionine *p*-toluenesulfonate salt [SAM], adenosine 5′-triphosphate disodium salt hydrate [ATP], DTT, pyridoxal 5′-phosphate hydrate [PLP], MgCl₂, NaHCO₃, bicine, and 1% w/v Igepal CA630) were obtained from Sigma-Aldrich, EMD Millipore,
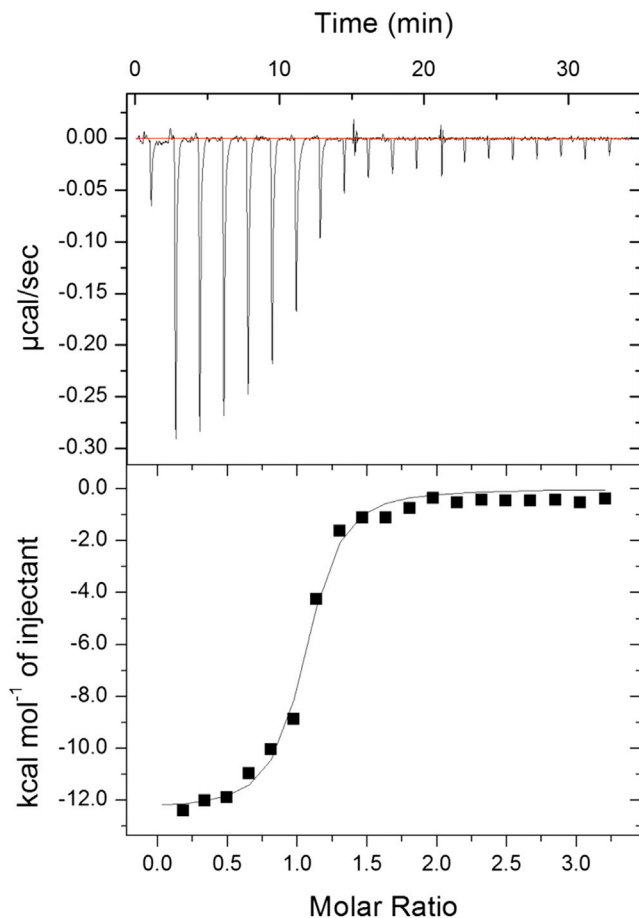
Figure 6. ITC Profile of 10 μM BioA with 103 μM 14

Experiments were performed as described in the Experimental Procedures. (Top) Data obtained from automatic titrations of 200 μl 14. (Bottom) The integrated curve showing experimental points (■) and the best fit (–). A fit of the data to a one-set-of-sites model produced the following values for the binding of 14 to BioA (average from duplicate experiments): n = 0.73 ± 0.11, $\Delta H = -11.8 \pm 0.8$ kcal mmol^{-1}, $-T\Delta S = 2.3 \pm 0.8$ kcal mol^{-1}; and $K_A = (9.23 \pm 0.89) \times 10^6$ M^{-1}.

or Fisher Scientific. *Mycobacterium tuberculosis* H37Rv, *Mycobacterium tuberculosis* SD1, and *Mycobacterium tuberculosis* SD5 strains have been described previously (Park et al., 2011). The reagents in Sauton's medium (0.5 g KH$_2$PO$_4$, 0.5 g MgSO$_4 \cdot$7H$_2$O, 2.0 g citric acid, 0.05 g ferric ammonium citrate, 60 ml glycerol, 4.0 g asparagine, 0.1 ml 1% ZnSO$_4$, and 0.02% tyloxapol in 1 l) for the *Mtb* whole-cell studies were obtained from Sigma-Aldrich. HEK293 (ATCC CRL-1573), HepG2 (ATCC HB-8065), and NIH 3T3 (ATCC CRL-1658) were obtained from the American Type Culture Collection, and cell culture medium and reagents (Dulbecco's modified Eagle's medium, fetal bovine serum, 0.25% trypsin-EDTA, Pen/Strep/L-Glutamine, and MG132) were purchased from Gibco. Mitoxantrone dihydrochloride was obtained from Enzo Life Sciences and the CellTiterGlo assay kit was purchased from Promega.

HTS Assay Protocol

Compounds in 10 mM DMSO stock solution (7.5 μL) were robotically dispensed into Aurora black 1,536-well plates (cat#00019180BX) using an Echo 555 acoustic liquid handler. The first and last four columns contained positive (compound CHM-1, CID357860) and negative (DMSO only) controls. Next, 3.75 μl reaction buffer (100 nM BioA, 640 nM BioD, 1.5 mM SAM, 20 mM

Fluorescent-DTB tracer 9, 92.5 nM streptavidin, 2 mM DTT, 5 mM ATP, 50 mM NaHCO$_3$, 1 mM MgCl$_2$, 0.1 mM PLP, 0.0025% Igepal CA630, and 100 mM Bicine [pH 8.6]) containing all reaction components except KAPA was dispensed into all wells of the plate. The reaction was started by the addition of 3.75 μl freshly prepared KAPA initiation solution (6 μM KAPA, 50 mM NaHCO$_3$, 1 mM MgCl$_2$, 0.0025% Igepal CA630, and 100 mM Bicine [pH 8.6]) and incubated at 25°C for 45 min. The reaction was terminated by the addition of 1.5 μl 500 mM EDTA into each well of the assay plate.

After 5 min equilibration, the plate was read on a Viewlux microplate reader in fluorescence mode with an excitation of 485 nM, an emission of 530 nM, and a cutoff of 530 nM (fluorescein isothiocyanate filters). The library was screened in duplicate and hits were procured as dry powders, and purity and structural assignment were verified by liquid chromatography-mass spectrometry analysis. Primary HTS data were analyzed in Genedata Screener Assay Analyzer. All values were normalized against DMSO-treated samples and the positive control. Z′ values were calculated for each plate from the positive and negative controls, and plates were considered technically acceptable for Z′-factors $\geq$ 0.75. For the HTS, the average of two replicates was used to rank order activity and to choose compounds for retests. A hit was defined when the average value of both replicates resulted in greater than 40% inhibition. The BioD counterscreen was performed analogously, but BioA was excluded from the reaction buffer, BioD was reduced to 10 nM (final concentration), and the reaction was initiated with DAPA initiation solution (8 μM DAPA, 50 mM NaHCO$_3$, 1 mM MgCl$_2$, 0.0025% Igepal CA630, and 100 mM Bicine [pH 8.6]). For dose-response studies, 2-fold dilutions of compound stock solutions were prepared from 10–0.078 mM in DMSO and 7.5 nl of these stock solutions were transferred to 1,536-well assay plates (as described above) to provide final compound concentrations in the well ranging from 10 to 0.078 μM. IC$_{50}$ curves were generated using a four-parameter Hill equation with the SmartFit algorithm in Genedata Screener version 7.0.3. The data were normalized to negative and positive controls as 0 and 100% inhibition, respectively, and the curves were then fit to the percentage activities.

Whole-Cell Screening Protocol

Mtb WT, BioA-UE, and BioA-OE were grown in Sauton's medium containing 1 μM biotin to an OD$_{580\,nm}$ between 1.0 and 1.2, harvested by centrifugation, washed twice with biotin-free Sauton's medium, and diluted in 96-well plates to an OD$_{580\,nm}$ of 0.03. The compounds were added to final concentrations between 50 and 0.2 μM. Wells containing no compound were used as controls. Biotin (1 μM) was added when indicated; 200 ng/ml anhydrotetracycline was added to the Mtb BioA-UE and BioA-OE to achieve the desired level of BioA expression. Plates were incubated at 37°C and optical density was measured after 14 days. All growth assays were performed in triplicate. MIC values were calculated using Prism (version 5.01).

Crystallization

BioA was cocrystallized with 14-Cl, 15, and 18 by the vapor-diffusion method in a hanging drop at 20°C, as previously described (Dai et al., 2014). Protein solution containing 10 mg/ml BioA in 25 mM HEPES (pH 7.5), 50 mM NaCl, 0.1 mM *tris*(2-carboxyethyl)phosphine (TCEP) was mixed with reservoir solution (9%–14% PEG 8000, 100 mM HEPES [pH 7.5], 100 mM MgCl$_2$, and 500 μM compound) and a seed solution (a reservoir solution containing crushed BioA crystals) in a 4:3:1 ratio (2 μl BioA protein:1.5 μl reservoir solution: 0.5 μl crushed BioA seed solution). Crystals appeared in the drop within 24 hr and grew to their full size in 72 hr. BioA-compound cocrystals were cryoprotected by transferring to a cryo solution (15% PEG 400, 15% PEG 8000, 100 mM HEPES [pH 7.5], 100 mM MgCl$_2$, and 5 mM compound) using an appropriately sized fiber loop of a cryo pin from Hampton Research and then flash frozen in liquid nitrogen.

Data Collection, Processing, and Model Building

The diffraction data for a cocrystal with 18 were collected at 100 K using Cu $K\alpha$ radiation on a Rigaku HighFlux HomeLab rotating-anode system with a Saturn 944+ CCD detector in the Kahlert Structural Biology Laboratory at the University of Minnesota. Diffraction data for 15 and 14-Cl, cocrystals were collected on a NOIR-1 CCD at ALS beamline 4.2.2. The data were processed, integrated, and scaled with d*TREK (Pflugrath, 1999). The structures

were solved by molecular replacement using Phaser (McCoy et al., 2007) in the CCP4 package (Winn et al., 2011) using atomic coordinates from Protein Data Bank (PDB) code 3TFT as a search model (Shi et al., 2011). Refinement and model building were done using REFMAC5 (Murshudov et al., 2011), PHENIX (Adams et al., 2010), and Coot (Emsley and Cowtan, 2004). Ligand geometry restraints were generated with PRODRG (Schüttelkopf and van Aalten, 2004). Figure 5 was prepared with PyMOL (PyMOL Molecular Graphics System, version 1.5.0.4, Schrödinger.) and Ligplot+ (Laskowski and Swindells, 2011). A summary of crystallographic data and refinement statistics is provided as Supplemental Information Table S2.

ITC

The ITC experiments were conducted on an automated microcalorimeter (Malvern Instruments). The experiments were performed at 25°C in ITC buffer (25 mM HEPES [pH 7.5] and 50 mM NaCl). BioA was exchanged (2 × 13 ml) into ITC buffer using an Amicon Ultra concentrator, and the final filtrate was used to prepare a solution of 14. In the titration experiments, 14 was injected into a solution of the enzyme. Ligand and protein concentrations were 10.2 μM for BioA (determined by Bradford analysis using BSA as a standard) and 103 μM for 14 (determined by weighing sample on a ultramicrobalance accurate to 0.001 mg). Titrations were carried out with a stirring speed of 750 rpm and 150 s interval between 4 μl injections. The first injection was excluded from data fitting. Titrations were run past the point of enzyme saturation to determine and correct for heats of dilution. The experimental data were fit to a theoretical titration curve using the Origin software package (version 7.0) provided with the instrument to afford values of K_A (the association constant in M^{-1}), n (the number of binding sites per monomer), and ΔH (the binding enthalpy change in kilocalories per mole). The thermodynamic parameters ΔG and ΔS were calculated using Equation 1 as follows:

$$\Delta G = -RT \ln K = \Delta H - T\Delta S, \qquad \text{(Equation 1)}$$

where ΔG, ΔH, and ΔS are the changes in free energy, enthalpy, and entropy of binding, respectively; $R = 1.98$ cal mol^{-1} K^{-1}; and T is the absolute temperature. The affinity of the ligand for the protein is given as the dissociation constant ($K_D = 1/K_A$). ITC experiments were performed in duplicate and analyzed independently, and the thermodynamic values obtained were averaged.

ACCESSION NUMBERS

Atomic coordinates have been deposited in the PDB with accession codes 4W1V, 4W1W, and 4W1X for complexes with 18, 15, and 14-Cl, respectively.

SUPPLEMENTAL INFORMATION

Supplemental Information includes Supplemental Experimental Procedures, one figure, and two tables and can be found with this article online at http://dx.doi.org/10.1016/j.chembiol.2014.11.012.

AUTHOR CONTRIBUTIONS

S.W.P. performed the whole-cell studies with *Mtb*. D.E.C. performed the primary HTS and secondary biochemical and cytotoxicity assays.

ACKNOWLEDGMENTS

REFERENCES

Abrahams, G.L., Kumar, A., Savvi, S., Hung, A.W., Wen, S., Abell, C., Barry, C.E., 3rd, Sherman, D.R., Boshoff, H.I., and Mizrahi, V. (2012). Pathway-selective sensitization of *Mycobacterium tuberculosis* for target-based whole-cell screening. Chem. Biol. *19*, 844–854.

Adams, P.D., Afonine, P.V., Bunkóczi, G., Chen, V.B., Davis, I.W., Echols, N., Headd, J.J., Hung, L.W., Kapral, G.J., Grosse-Kunstleve, R.W., et al. (2010). PHENIX: a comprehensive Python-based system for macromolecular structure solution. Acta Crystallogr. D Biol. Crystallogr. *66*, 213–221.

Aldrich, C.C., Boshoff, H.I., and Remmel, R.P. (2010). Antitubercular agents. In Burgers Medicinal Chemistry, Drug Discovery, and Development, Seventh Edition, D. Rotella and D.J. Abraham, eds. (Hoboken: John Wiley & Sons), pp. 713–812.

Andries, K., Verhasselt, P., Guillemont, J., Göhlmann, H.W., Neefs, J.M., Winkler, H., Van Gestel, J., Timmerman, P., Zhu, M., Lee, E., et al. (2005). A diarylquinoline drug active on the ATP synthase of *Mycobacterium tuberculosis*. Science *307*, 223–227.

Baell, J.B., and Holloway, G.A. (2010). New substructure filters for removal of pan assay interference compounds (PAINS) from screening libraries and for their exclusion in bioassays. J. Med. Chem. *53*, 2719–2740.

Centers for Disease Control and Prevention (CDC) (1999). Control of infectious diseases. MMWR Morb. Mortal. Wkly. Rep. *48*, 621–629.

Copeland, R.A. (2000). Enzymes: A Practical Introduction to Structure, Mechanism and Data Analysis. (New York: John Wiley & Sons).

Dai, R., Wilson, D.J., Geders, T.W., Aldrich, C.C., and Finzel, B.C. (2014). Inhibition of *Mycobacterium tuberculosis* transaminase BioA by aryl hydrazines and hydrazides. ChemBioChem *15*, 575–586.

DeVito, J.A., Mills, J.A., Liu, V.G., Agarwal, A., Sizemore, C.F., Yao, Z., Stoughton, D.M., Cappiello, M.G., Barbosa, M.D., Foster, L.A., and Pompliano, D.L. (2002). An array of target-specific screening strains for antibacterial discovery. Nat. Biotechnol. *20*, 478–483.

Dey, S., Lane, J.M., Lee, R.E., Rubin, E.J., and Sacchettini, J.C. (2010). Structural characterization of the *Mycobacterium tuberculosis* biotin biosynthesis enzymes 7,8-diaminopelargonic acid synthase and dethiobiotin synthetase. Biochemistry *49*, 6746–6760.

Edfeldt, F.N., Folmer, R.H., and Breeze, A.L. (2011). Fragment screening to predict druggability (ligandability) and lead discovery success. Drug Discov. Today *16*, 284–287.

Emsley, P., and Cowtan, K. (2004). Coot: model-building tools for molecular graphics. Acta Crystallogr. D Biol. Crystallogr. *60*, 2126–2132.

Forsyth, R.A., Haselbeck, R.J., Ohlsen, K.L., Yamamoto, R.T., Xu, H., Trawick, J.D., Wall, D., Wang, L., Brown-Driver, V., Froelich, J.M., et al. (2002). A genome-wide strategy for the identification of essential genes in *Staphylococcus aureus*. Mol. Microbiol. *43*, 1387–1400.

Geders, T.W., Gustafson, K., and Finzel, B.C. (2012). Use of differential scanning fluorimetry to optimize the purification and crystallization of PLP-dependent enzymes. Acta Crystallogr. Sect. F Struct. Biol. Cryst. Commun. *68*, 596–600.

Gerard, B., Duvall, J.R., Lowe, J.T., Murillo, T., Wei, J., Akella, L.B., and Marcaurelle, L.A. (2011). Synthesis of a stereochemically diverse library of medium-sized lactams and sultams via S(N)Ar cycloetherification. ACS Comb. Sci. *13*, 365–374.

Gerard, B., O'Shea, M.W., Donckele, E., Kesavan, S., Akella, L.B., Xu, H., Jacobsen, E.N., and Marcaurelle, L.A. (2012). Application of a catalytic asymmetric Povarov reaction using chiral ureas to the synthesis of a tetrahydroquinoline library. ACS Comb. Sci. *14*, 621–630.

Gerard, B., Lee, M.D., 4th, Dandapani, S., Duvall, J.R., Fitzgerald, M.E., Kesavan, S., Lowe, J.T., Marié, J.C., Pandya, B.A., Suh, B.C., et al. (2013). Synthesis of stereochemically and skeletally diverse fused ring systems from functionalized C-glycosides. J. Org. Chem. *78*, 5160–5171.

Gopal, P., and Dick, T. (2014). Reactive dirty fragments: implications for tuberculosis drug discovery. Curr. Opin. Microbiol. *21C*, 7–12.

Kitahara, T., Hotta, K., Yoshida, M., and Okami, Y. (1975). Biological studies of amiclenomycin. J. Antibiot. *28*, 215–221.

Laskowski, R.A., and Swindells, M.B. (2011). LigPlot+: multiple ligand-protein interaction diagrams for drug discovery. J. Chem. Inf. Model. *51*, 2778–2786.

Lee, R.E., Hurdle, J.G., Liu, J., Bruhn, D.F., Matt, T., Scherman, M.S., Vaddady, P.K., Zheng, Z., Qi, J., Akbergenov, R., et al. (2014). Spectinamides: a new class of semisynthetic antituberculosis agents that overcome native drug efflux. Nat. Med. *20*, 152–158.

Lin, S., Hanson, R.E., and Cronan, J.E. (2010). Biotin synthesis begins by hijacking the fatty acid synthetic pathway. Nat. Chem. Biol. *6*, 682–688.

Lowe, J.T., Lee, M.D., 4th, Akella, L.B., Davoine, E., Donckele, E.J., Durak, L., Duvall, J.R., Gerard, B., Holson, E.B., Joliton, A., et al. (2012). Synthesis and profiling of a diverse collection of azetidine-based scaffolds for the development of CNS-focused lead-like libraries. J. Org. Chem. *77*, 7187–7211.

Mann, S., and Ploux, O. (2006). 7,8-Diaminoperlargonic acid aminotransferase from *Mycobacterium tuberculosis*, a potential therapeutic target. Characterization and inhibition studies. FEBS J. *273*, 4778–4789.

Mann, S., and Ploux, O. (2011). Pyridoxal-5′-phosphate-dependent enzymes involved in biotin biosynthesis: structure, reaction mechanism and inhibition. Biochim. Biophys. Acta *1814*, 1459–1466.

Mann, S., Colliandre, L., Labesse, G., and Ploux, O. (2009). Inhibition of 7,8-diaminopelargonic acid aminotransferase from *Mycobacterium tuberculosis* by chiral and achiral anologs of its substrate: biological implications. Biochimie *91*, 826–834.

Mann, S., Eveleigh, L., Lequin, O., and Ploux, O. (2013). A microplate fluorescence assay for DAPA aminotransferase by detection of the vicinal diamine 7,8-diaminopelargonic acid. Anal. Biochem. *432*, 90–96.

Marcaurelle, L.A., Johannes, C., Yohannes, D., Tillotson, B.P., and Mann, D. (2009). Diversity-oriented synthesis of a cytisine-inspired pyridone library leading to the discovery of novel inhibitors of Bcl-2. Bioorg. Med. Chem. Lett. *19*, 2500–2503.

Marriner, G.A., Nayyar, A., Uh, E., Wong, S.Y., Mukherjee, T., Via, L.E., Carroll, M., Edwards, R.L., Gruber, T.D., Choi, I., et al. (2011). The medicinal chemistry of tuberculosis chemotherapy. Top. Med. Chem. *7*, 47–124.

McCoy, A.J., Grosse-Kunstleve, R.W., Adams, P.D., Winn, M.D., Storoni, L.C., and Read, R.J. (2007). Phaser crystallographic software. J. Appl. Cryst. *40*, 658–674.

McGovern, S.L., Helfand, B.T., Feng, B., and Shoichet, B.K. (2003). A specific mechanism of nonspecific inhibition. J. Med. Chem. *46*, 4265–4272.

Mulrooney, C.A., Lahr, D.L., Quintin, M.J., Youngsaye, W., Moccia, D., Asiedu, J.K., Mulligan, E.L., Akella, L.B., Marcaurelle, L.A., Montgomery, P., et al. (2013). An informatic pipeline for managing high-throughput screening experiments and analyzing data from stereochemically diverse libraries. J. Comput. Aided Mol. Des. *27*, 455–468.

Murshudov, G.N., Skubák, P., Lebedev, A.A., Pannu, N.S., Steiner, R.A., Nicholls, R.A., Winn, M.D., Long, F., and Vagin, A.A. (2011). REFMAC5 for the refinement of macromolecular crystal structures. Acta Crystallogr. D Biol. Crystallogr. *67*, 355–367.

NIH (2014). NIH fact sheet: tuberculosis. http://report.nih.gov/nihfactsheets/ViewFactSheet.aspx?csid=31.

Palmer, A.C., and Kishony, R. (2014). Opposing effects of target overexpression reveal drug mechanisms. Nat. Commun. *5*, 4296.

Park, S.W., Klotzsche, M., Wilson, D.J., Boshoff, H.I., Eoh, H., Manjunatha, U., Blumenthal, A., Rhee, K., Barry, C.E., 3rd, Aldrich, C.C., et al. (2011). Evaluating the sensitivity of *Mycobacterium tuberculosis* to biotin deprivation using regulated gene expression. PLoS Pathog. *7*, e1002264.

Payne, D.J., Gwynn, M.N., Holmes, D.J., and Pompliano, D.L. (2007). Drugs for bad bugs: confronting the challenges of antibacterial discovery. Nat. Rev. Drug Discov. *6*, 29–40.

Pflugrath, J.W. (1999). The finer things in X-ray diffraction data collection. Acta Crystallogr. D Biol. Crystallogr. *55*, 1718–1725.

Phillips, J.W., Goetz, M.A., Smith, S.K., Zink, D.L., Polishook, J., Onishi, R., Salowe, S., Wiltsie, J., Allocco, J., Sigmund, J., et al. (2011). Discovery of kibdelomycin, a potent new class of bacterial type II topoisomerase inhibitor by chemical-genetic profiling in *Staphylococcus aureus*. Chem. Biol. *18*, 955–965.

Sandmark, J., Mann, S., Marquet, A., and Schneider, G. (2002). Structural basis for the inhibition of the biosynthesis of biotin by the antibiotic amiclenomycin. J. Biol. Chem. *277*, 43352–43358.

Schatz, A., Bugle, E., and Waksman, S.A. (1944). Streptomycin, a substance exhibiting antibiotic activity against Gram-positive and Gram-negative bacteria. Exp. Biol. Med. *55*, 66–69.

Schüttelkopf, A.W., and van Aalten, D.M. (2004). PRODRG: a tool for high-throughput crystallography of protein-ligand complexes. Acta Crystallogr. D Biol. Crystallogr. *60*, 1355–1363.

Shapiro, M.M., Chakravartty, V., and Cronan, J.E. (2012). Remarkable diversity in the enzymes catalyzing the last step in synthesis of the pimelate moiety of biotin. PLoS ONE *7*, e49440.

Shi, C., Geders, T.W., Park, S.W., Wilson, D.J., Boshoff, H.I., Abayomi, O., Barry, C.E., 3rd, Schnappinger, D., Finzel, B.C., and Aldrich, C.C. (2011). Mechanism-based inactivation by aromatization of the transaminase BioA involved in biotin biosynthesis in *Mycobaterium tuberculosis*. J. Am. Chem. Soc. *133*, 18194–18201.

Silver, L.L. (2011). Challenges of antibacterial discovery. Clin. Microbiol. Rev. *24*, 71–109.

Silver, L.L. (2013). Viable screening targets related to the bacterial cell wall. Ann. N Y Acad. Sci. *1277*, 29–53.

Vasanthakumar, G.R., Bhor, V.M., and Surolia, A. (2007). Hydrolysis of cyclic ureas under microwave irradiation: synthesis and characterization of 7,8-diaminopelargonic acid. Synth. Commun. *37*, 2633–2639.

Wang, J., Soisson, S.M., Young, K., Shoop, W., Kodali, S., Galgoci, A., Painter, R., Parthasarathy, G., Tang, Y.S., Cummings, R., et al. (2006). Platensimycin is a selective FabF inhibitor with potent antibiotic properties. Nature *441*, 358–361.

Wilson, D.J., Shi, C., Duckworth, B.P., Muretta, J.M., Manjunatha, U., Sham, Y.Y., Thomas, D.D., and Aldrich, C.C. (2011). A continuous fluorescence displacement assay for BioA: an enzyme involved in biotin biosynthesis. Anal. Biochem. *416*, 27–38.

Winn, M.D., Ballard, C.C., Cowtan, K.D., Dodson, E.J., Emsley, P., Evans, P.R., Keegan, R.M., Krissinel, E.B., Leslie, A.G., McCoy, A., et al. (2011). Overview of the CCP4 suite and current developments. Acta Crystallogr. D Biol. Crystallogr. *67*, 235–242.

World Health Organization (WHO) (2013). Global Tuberculosis Report 2013. (Geneva: WHO Press).

Yin, D., Fox, B., Lonetto, M.L., Etherton, M.R., Payne, D.J., Holmes, D.J., Rosenberg, M., and Ji, Y. (2004). Identification of antimicrobial targets using a comprehensive genomic approach. Pharmacogenomics *5*, 101–113.

Young, K., Jayasuriya, H., Ondeyka, J.G., Herath, K., Zhang, C., Kodali, S., Galgoci, A., Painter, R., Brown-Driver, V., Yamamoto, R., et al. (2006). Discovery of FabH/FabF inhibitors from natural products. Antimicrob. Agents Chemother. *50*, 519–526.

Zhang, J.H., Chung, T.D., and Oldenburg, K.R. (1999). A simple statistical parameter for use in evaluation and validation of high throughput screening assays. J. Biomol. Screen. *4*, 67–73.

Zlitni, S., Ferruccio, L.F., and Brown, E.D. (2013). Metabolic suppression identifies new antibacterial inhibitors under nutrient limitation. Nat. Chem. Biol. *9*, 796–804.